Spin transport in fully hexagonal boron nitride encapsulated graphene

M. Gurram,[1,][*] S. Omar,[1] S. Zihlmann,[2] P. Makk,[2] C. Schönenberger,[2] and B. J. van Wees[1]

[1]*Physics of Nanodevices, Zernike Institute for Advanced Materials, University of Groningen, The Netherlands*
[2]*Department of Physics, University of Basel, Basel, Switzerland*

We study fully hexagonal boron nitride (hBN) encapsulated graphene spin valve devices at room temperature. The device consists of a graphene channel encapsulated between two crystalline hBN flakes: thick-hBN flake as a bottom gate dielectric substrate which masks the charge impurities from SiO$_2$/Si substrate and single-layer thin-hBN flake as a tunnel barrier. Full encapsulation prevents the graphene from coming in contact with any polymer/chemical during the lithography and thus gives homogeneous charge and spin transport properties across different regions of the encapsulated graphene. Further, even with the multiple electrodes in-between the injection and the detection electrodes which are in conductivity mismatch regime, we observe spin transport over 12.5-μm-long distance under the thin-hBN encapsulated graphene channel, demonstrating the clean interface and the pinhole-free nature of the thin hBN as an efficient tunnel barrier.

I. INTRODUCTION

Graphene is considered as an ideal material for spintronics due to its low intrinsic spin-orbit coupling, small hyperfine interaction, tunable carrier density, and high electron mobility [1–3] even at room temperature, which is important for future applications. Theoretically, it is estimated to show long spin relaxation length (λ_s) of 100 μm and high spin relaxation time (τ_s) of 100 ns [4,5]. At the moment, experimentally these values are reported up to $\lambda_s = 30.5$ μm and $\tau_s = 12.6$ ns [6]. In a quest to figure out the sources limiting the intrinsic spin transport in graphene, there have been several experiments, which suggest that the role of underlying substrate and the quality of tunnel barrier is crucial [7].

The quality of substrate plays an important role in determining the charge and the spin transport characteristics of graphene. An atomically flat hexagonal boron nitride (hBN) substrate has shown to provide a good base for high mobility graphene [8] and long spin relaxation length [9] because hBN has less charged impurities and the thickness of the bottom hBN moves the graphene away from the charged impurities in the SiO$_2$ substrate. Also, the effect of the electron-hole puddles can be different for different substrates and it is lower with a hBN substrate [10].

Recently, Kretinin *et al.* [11] demonstrated the high electronic quality of graphene by encapsulating it from surroundings with different two-dimensional (2D) crystals such as hBN and transition-metal dichalcogenide (TMD). However, this device geometry comprised of one-dimensional edge electrodes [8] with a thick semiconducting TMD top layer which is not compatible for standard four-probe nonlocal spin transport measurements. In this work, we replace the TMD with an atomically thin-hBN flake, which serves two purposes. First, it acts as an encapsulating layer. Second, it acts as a tunnel barrier replacing the conventional oxide tunnel barrier. Therefore, it allows to probe the charge and the spin transport properties of the encapsulated graphene with multiple ferromagnetic (FM) electrodes.

The previous studies have shown that the graphene interface with spin-sensitive ferromagnetic electrodes affects the spin transport behavior. Further, the conventional oxide tunnel barriers used in spintronic devices suffer from pinholes, inhomogeneous coverage, nonuniform growth, and consequently contributing to the low spin transport properties [7,12]. A 2D layer of thin hBN with close lattice match to graphene has been shown to exhibit pinhole-free tunneling characteristics [13,14]. It is also predicted to enhance the spin injection efficiency from a ferromagnet into graphene [15].

Yamaguchi *et al.* [16] first reported spin injection through exfoliated monolayer hBN tunnel barrier into bilayer graphene resulting in quite low spin transport parameters ($\tau_s = 56$ ps, $D_s = 0.034$ m^2/s, $\lambda_s = 1.35$ μm) and low mobility ($\mu = 2700$ cm^2/Vs) of graphene. Further, Kamalakar *et al.* [17] and Fu *et al.* [18] used large-scale chemical vapor deposited (CVD) bilayer hBN tunnel barriers for spin injection into graphene. The spin polarization increased with CVD hBN barriers. However, the quality of graphene channel is limited by the wet transfer technique used for transferring CVD hBN on to graphene. In contrast, we use a dry pickup and transfer technique [19] in order to completely cover the underlying graphene with a thin-hBN flake, which acts a tunnel barrier and also shields the graphene from external polymers and chemicals during the lithography process.

It is also worth discussing here that the previous reports on spin transport in hBN encapsulated graphene are quite promising in terms of improved spin transport parameters [20,21]. However, extracting the correct spin transport parameters is not straightforward due to inhomogeneous spin transport behavior of the hBN encapsulated and the non-hBN encapsulated graphene regions. A similar behavior is also observed for partly suspended high mobility graphene [22]. Using our device geometry, we can achieve more homogeneous charge and spin transport behavior in the graphene channel compared to the previously reported results.

In this work, we report a fully hBN encapsulated graphene spintronics device to overcome the three aforementioned challenges, namely, (1) the influence of underlying substrate, (2) the influence of tunnel barrier interface, and (3) the inhomogeneity in graphene channel. We use a dry pickup

———————
[*]Corresponding author: m.gurram@rug.nl

technique which prevents the graphene from external doping
and results in more homogeneous charge and spin transport
parameters at room temperature.

II. DEVICE FABRICATION

The hBN/graphene/hBN stack is prepared following the
dry pickup and transfer technique [8,19]. The graphene and
hBN flakes were obtained by the exfoliation of highly oriented
pyrolytic graphite (HOPG, SPI Supplies, ZYA grade) and hBN
powder (HQ graphene). A 90-nm-thick SiO_2/Si substrate is
used for exfoliation and identification of graphene and thin-
hBN flakes as it gives a good optical contrast to search for thin-
ner graphene [23] and hBN [24] flakes down to a monolayer.

A polydimethylsiloxane (PDMS) polymer stamp prepared
with polycarbonate (PC) layer is used to pick up the flakes.
At first, a glass substrate with PDMS/PC is used to pick up
a thick top-hBN flake which is used to pick up the thin-hBN
flake followed by picking up the graphene flake. Then, the
PC/top-hBN/thin-hBN/graphene stack is released onto a thick
bottom hBN on a SiO_2(300 nm)/Si substrate by melting the
PC layer. Next, the PC layer is dissolved in chloroform for
5 h at $50\,^{\circ}$C, followed by annealing in Ar/H_2 atmosphere at
$350\,^{\circ}$C for 12 h to remove the leftover PC residues on top of
the thin hBN and the top hBN. It is important to note that the
graphene beneath the thin hBN does not come in contact with
polymers during the fabrication due to the full encapsulation
by hBN flakes.

Thereafter, electron-beam lithography is used for pattern-
ing of electrodes on the poly(methylmethacrylate) (PMMA)
coated stack followed by electron-beam evaporation to deposit
65 nm of ferromagnetic cobalt (Co) for spin-sensitive elec-
trodes. Cobalt is capped with 4-nm-thick aluminum (Al) layer
to prevent it from oxidation. A schematic of the layer-by-layer
device structure is shown in Fig. 1(a).

An optical micrograph of the fabricated device is shown
in Fig. 1(b) where the graphene and the thin-hBN flakes are
outlined with the black and the white dashed lines, respectively.
Due to a slight misalignment during the pickup process, a
region of 0.1–0.2 μm width along the top edge of the graphene
flake is not covered by the thin hBN. However, the electrodes
in-between E2 and E5 are deposited on top of the thin-hBN
layer, avoiding the uncovered top-edge graphene region. The
thin-hBN encapsulated graphene does not come in contact with
polymers whereas the graphene regions which are not covered
by the thin hBN are touched by PC and PMMA polymers
during the fabrication.

We performed atomic force microscopy (AFM) imaging to
find the thickness of each flake used in the device fabrication.
It is found to be 0.40 nm for graphene and 0.52 nm for
thin-hBN layer. These values are in close agreement with
the experimentally reported thickness for single-layer (1L)-
graphene [25] and 1L-hBN [14,17].

III. RESULTS AND DISCUSSION

We report the measurements for the different regions of
fully encapsulated graphene channel as labeled in the optical
image shown in Fig. 1(b). Specifically, Ch1 (4.5 μm, between
E2 and E3) and Ch3 (3 μm, between E4 and E5) regions consist
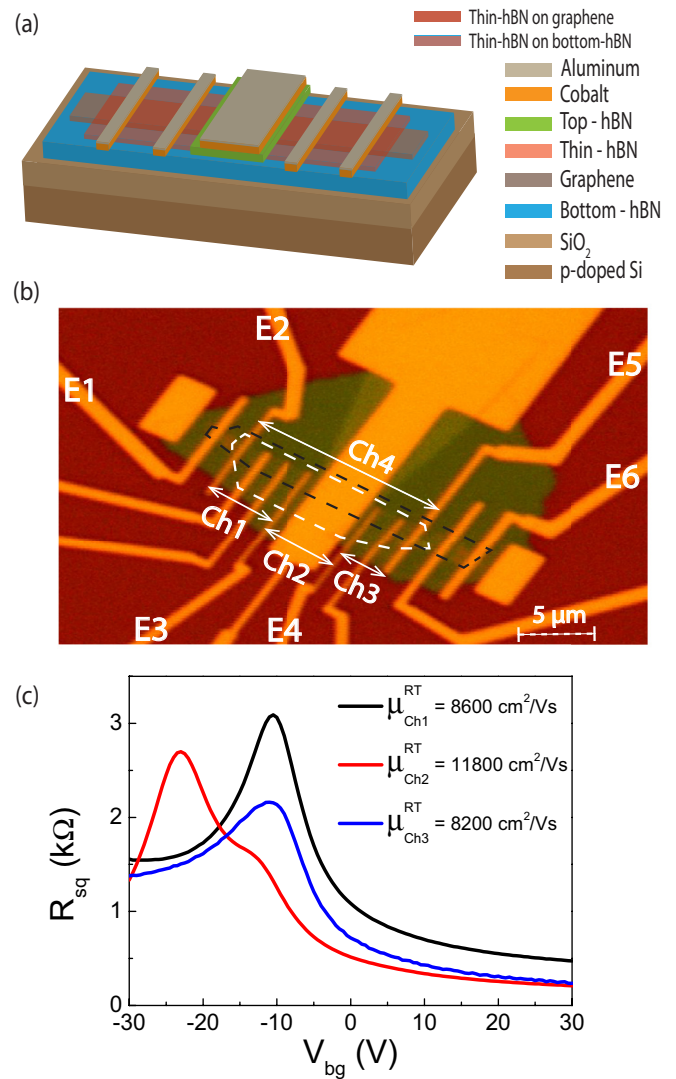of graphene encapsulated by thin hBN. Ch2 (5 μm, between

FIG. 1. (a) Schematic of the proposed fully hBN encapsulated
graphene spin valve device. (b) An optical microscope image of
the fabricated device on SiO_2(300 nm)/Si substrate with multiple
ferromagnetic cobalt electrodes (65 nm) with aluminum capping layer
(4 nm) denoted as E(1–6). The graphene flake (0.4 nm) is completely
supported underneath by the thick bottom hBN (21 nm) flake and
encapsulated by the thin-hBN (0.52 nm) layer between the electrodes
E2 and E5. The different regions of the thin-hBN encapsulated
graphene channel are denoted as Ch(1–4) with the double arrows. The
boundaries of graphene and thin-hBN flakes are outlined with black
and white dashed lines, respectively. (c) Room-temperature square
resistance (R_{sq}) for different graphene channel regions as a function
of backgate voltage (V_{bg}). The corresponding electron mobility values
are given in the legend.

E3 and E4) region comprised of graphene encapsulated by
the thin hBN. On top of the thin hBN, we put thick top-hBN
(6-nm) flake which serves as a topgate dielectric. Finally, Ch4
(12.5 μm, between E2 and E5) consists of region across the
whole thin-hBN encapsulated graphene.

The resistance area product ($R_c A$) for graphene/hBN/
graphene tunnel junction is reported to scale exponentially
with the number of hBN layers [14]. We characterize the thin-
hBN/graphene interface resistance (R_c) using a three-probe

measurement scheme. The $R_c A$ product for the electrodes E(2-5) is found to be in the range of 0.3–1.1 k$\Omega\,\mu$m^2 which agrees with the reported values for single-layer hBN tunnel barriers [14,17,18]. Both the AFM and the $R_c A$ analysis confirm the single-layer nature of the thin-hBN flake.

All the measurements are carried out at room temperature in a vacuum of 10^{-6} mbar. Charge transport measurements are carried out in a local four-probe measurement scheme. An ac current is passed between electrodes E1 and E6 [Fig. 1(b)], and the voltage drop is measured across the electrodes for different transport channel regions in-between. The measured square resistance (R_{sq}) is presented in Fig. 1(c) for three different graphene channel regions Ch1, Ch2, and Ch3. The square resistance for the thin-hBN encapsulated regions [in Ch(1–3)] shows charge neutrality point (CNP) around -12 V and for the top-hBN encapsulated part of the Ch2 region show it around -23 V. A small bump at -12 V in R_{sq} data for Ch2 region corresponds to the thin-hBN encapsulated parts on either side of the top hBN.

The field effect mobility (μ) of graphene channel is calculated by fitting the R_{sq} data [Fig. 1(c)] using the relation $R_{sq} = 1/(ne\mu + \sigma_0) + \rho_s$, where e is the electronic charge, n is the carrier density, σ_0 is the residual conductivity at the CNP, and ρ_s is the contribution from short-range scattering [26,27]. The fitted values of the electron mobility for three different regions are $\mu_{Ch1} = 8600$ cm^2/Vs, $\mu_{Ch2} = 11\,800$ cm^2/Vs, and $\mu_{Ch3} = 8200$ cm^2/Vs. The close values of mobility at different regions reflect that the graphene channel is homogeneous under the thin-hBN encapsulation. A relatively higher value of mobility for Ch2 region is attributed to the central top-hBN encapsulated graphene while the remaining thin-hBN encapsulated graphene (Ch1 and Ch3) on either side of top hBN has an uncovered graphene edge of 0.1–0.2 μm width which are exposed to polymers during the fabrication.

The spin transport measurements are performed in a four-probe nonlocal geometry [Fig. 2(a)] at room temperature using standard ac lock-in technique with currents of 10–20 μA. We inject a spin polarized current using an ac current source (I_{ac}) and measure the nonlocal voltage (V_{nl}) while sweeping an in-plane magnetic field (B_y) parallel to the long axis of the ferromagnetic electrodes. The width of the electrodes is varied from 0.2 to 0.8 μm in order to switch magnetization of the electrodes at different coercive fields. As the B_y is swept from a negative magnetic field to a positive field, steps in $R_{nl}(=V_{nl}/I_{ac})$ are observed whenever the magnetization of the two inner electrodes changes between parallel and antiparallel configurations. The influence of the outer electrodes will be diminished if chosen far from the injection/detection electrodes, resulting in a typical two-level spin valve signal. In order to assess the spin transport nature of graphene, we extract the spin relaxation parameters from the Hanle spin precession measurements.

Hanle measurements are carried out in a four-probe nonlocal spin valve geometry as shown in Fig. 2(a) while the magnetic field is applied perpendicular (B_z) to the device plane. As the polarization of the injected spins is along the y direction, B_z causes the spins to precess in x-y plane with a Larmor frequency $\omega_L = g_e \mu_B B_z/\hbar$, where the Lande g factor $g = 2$, μ_B the Bohr magneton, and $\hbar$ the reduced Plank constant. In order to eliminate the background magnetore-
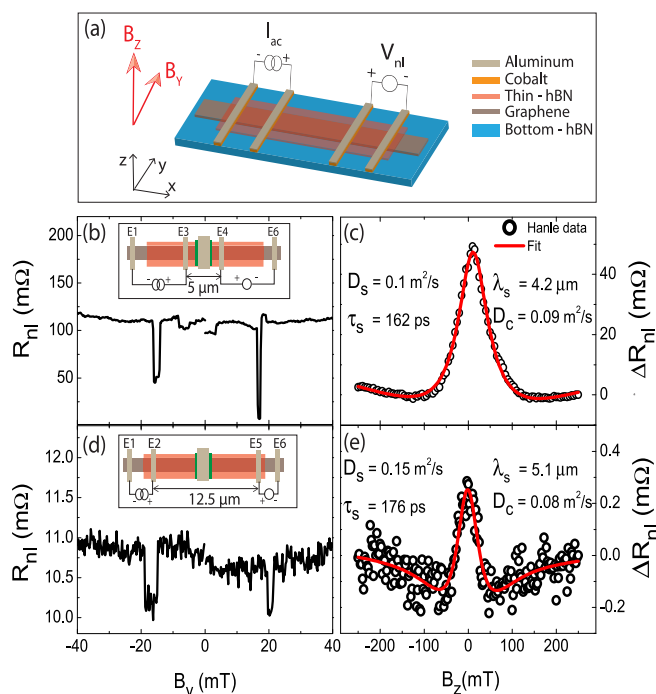

FIG. 2. (a) Schematic of the four-probe nonlocal geometry for the spin valve and the Hanle measurements. Spin valve signals measured at $V_{bg} = 30$ V for the top-hBN encapsulated (Ch2, between electrodes E3 and E4) region (b), and across the whole thin-hBN encapsulated (Ch4, between electrodes E2 and E5) region (d). The corresponding Hanle signals and fitting curves (c) and (e). The insets in (b) and (d) show the measurement geometry and the length of the graphene channel.

sistance effects, we analyze the effective Hanle spin signal $\Delta R_{nl} = (R_{nl}^{\uparrow\uparrow} - R_{nl}^{\uparrow\downarrow})/2$, where $R_{nl}^{\uparrow\uparrow(\uparrow\downarrow)}$ is the Hanle signal for the parallel (antiparallel) magnetization configuration of the injection and the detection electrodes. The resulting precession data ΔR_{nl} are fitted with the stationary solutions to the 1D Bloch equation in the diffusion regime; $D_s \nabla^2 \vec{\mu}_s - \vec{\mu}_s/\tau_s + \vec{\omega}_L \times \vec{\mu}_s = 0$, where μ_s is the spin chemical potential, D_s is the spin diffusion constant, and τ_s is the spin relaxation time.

The spin valve signals for the Ch2 region and across the whole thin-hBN encapsulated (Ch4) region are shown in Figs. 2(b) and 2(d), measured at the backgate voltage of 30 V. The corresponding Hanle signals and their fitting curves are shown in Figs. 2(c) and 2(e).

The extracted value of τ_s for different channel regions [Ch(1–4)] is in the range of 135–176 ps, D_s is of 0.11–0.18 m^2/s, and the corresponding value of the spin relaxation length $\lambda_s (=\sqrt{D_s\tau_s})$ is of 4.2–5.1 μm. The charge diffusion coefficient (D_c) calculated from the resistivity (R_{sq}) data in Fig. 1(c) is in the range of 0.07–0.09 m^2/s. As the values of D_c and D_s are in a reasonable agreement, we confirm the reliability of Hanle fitting [22,28].

As we can see from the Hanle fitting data [Figs. 2(c) and 2(e)], the spin relaxation parameters do not differ much for different encapsulated regions under thin hBN. Besides, the mobility values also lie close to each other [Fig. 1(c)]. It indicates that a consistent charge and spin transport behavior is observed across different regions of the thin-hBN encapsulated graphene.

The values of spin relaxation parameters are quite low compared to the graphene on hBN [9] or even partly encapsulated by hBN [20]. The thin-hBN flake is of single layer and it resulted in low interface resistance (R_c) values for the electrodes E(2–5), 0.6–2.1 kΩ which lie in the same order of the spin resistance (R_λ) for the thin-hBN encapsulated graphene, 0.4–1.4 kΩ where $R_\lambda = R_{sq}\lambda_s/W$, $W = 1.8$ μm is the width of the graphene. These values imply that the device is within the conductivity mismatch regime [28]. A similar behavior is also reported by Yamaguchi *et al.* [16] with exfoliated 1L-hBN and Fu *et al.* [18] with CVD 1L-hBN tunnel barriers.

It is also important to note in our device that the ferromagnetic cobalt electrodes on top of the thin-hBN layer are deposited in order to avoid contact with the uncovered (by thin-hBN) graphene edge [Fig. 1(b)]. The proximity of the stray magnetic field from the ends of the cobalt electrodes (between E2 and E5) can act as an additional dephasing field and influence the spin transport in graphene. Also, the uncovered region is exposed to the PC and PMMA polymers during the fabrication which can reduce the mobility and spin relaxation time.

Further, we would like to emphasize that the spin diffusion is detected across 12.5-μm length of thin-hBN encapsulated (Ch4) graphene region [Figs. 2(d) and 2(e)] which consists of multiple electrodes in-between the spin injection (E2) and the spin detection (E5) electrodes [Fig. 1(b)]. The conventional oxide-barrier/graphene interfaces are reported to act as spin sinks especially when their R_c lie close to R_λ [12,28,29] which hinders the long distance spin transport in graphene with multiple electrodes. Whereas, within the conductivity mismatched regime, our device still performs better than the device with oxide barriers, which might have pinholes. Hence, we attribute the observed long distance spin transport behavior to the pinhole-free nature of the thin-hBN layer and to the clean interface of thin hBN with the graphene compared to the deposited oxide tunnel barrier.

We would also like to point out that we do not observe the very long spin relaxation length or high spin relaxation time as in the case of partly hBN encapsulated graphene stack reported by Guimarães *et al.* [20], and it is worthwhile to mention the differences between our device and the stack reported in Ref. [20]. In our device, PMMA residues lie at the thin-hBN/cobalt electrode interface which might affect the spin injection/detection in a different way than in the stack reported in Ref. [20], which has PMMA residues between the graphene and the oxide tunnel barrier. Further, our device shows lower mobility and charge diffusion constant which also translates to the lower spin relaxation length.

Furthermore, using our device structure we can control the electric field and the carrier density independently with the top and the bottom gate electrodes. This allows us to study (i) the electrical control of spin information in graphene [20], and (ii) the spin transport across the p/n junctions created by the topgate and the nontopgate encapsulated graphene. It is interesting to study the spin transport across the p/n junction, which acts as a barrier for the transmission of spins, and results in high magnetoresistance and sensitivity in a spin valve transistor [30].
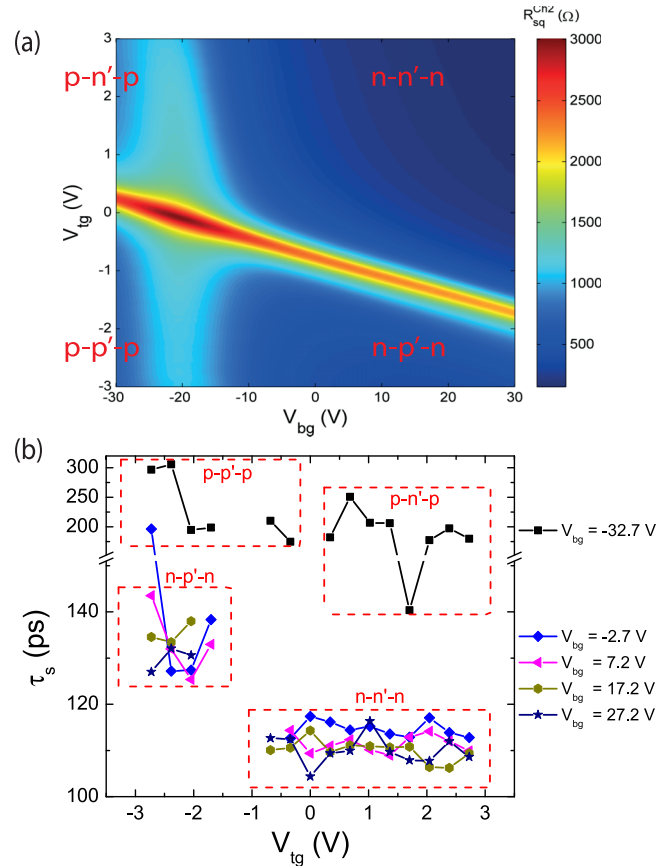

FIG. 3. (a) Contour plot of square resistance R_{sq} for top-hBN encapsulated (Ch2) region measured at room temperature with respect to backgate (V_{bg}) and topgate (V_{tg}) voltages. The polarities p or n (p' or n') type of nontopgated (topgated) encapsulated regions are tuned independently using the combinations of V_{bg} and V_{tg} which resulted in n-n'-n, n-p'-n, p-n'-p, and p-p'-p junction configurations. (b) Spin relaxation time as a function of topgate voltage at different backgate voltages. The dashed red lines outline the data corresponding to the four junction configurations.

A contour plot for the square resistance of the Ch2 region (R_{sq}^{Ch2}) as a function of topgate voltage V_{tg} and backgate voltage V_{bg} is shown in Fig. 3(a). The charge neutrality point (CNP) appears as a line with a slope of -0.034 which is equivalent to the ratio of the top and bottom gate dielectric capacitances. The maximum R_{sq} of the CNP appears at $V_{bg} \approx -22.7$ V, $V_{tg} \approx 0$ V and decreases along either side of the line. It is a characteristic behavior observed with single-layer graphene [20]. The V_{tg} independent feature around $V_{bg} = -22.7$ V appears due to the sides of the top-hBN encapsulated region that are nontopgated between the electrodes E3 and E4 [21].

We can create an effective electric field in the top-hBN encapsulated part of the Ch2 region by modulating the topgate voltage and the backgate voltage [31]. The perpendicular electric field can induce a Rashba spin orbit field in graphene [20] which can be used to manipulate the spin transport properties of the topgate encapsulated graphene channel.

The maximum value of the electric field created within the range of applied V_{tg} and V_{bg} is 0.22 V/nm. We do not observe a significant dependence of the spin relaxation time on the

electric field. We attribute this to the lower field compared to the Rashba field (0.7 V/nm) applied in the case of Guimarães *et al.* [20].

Within the Ch2 region, carrier density in the nontopgate encapsulated parts is controlled by V_{bg} whereas the central topgate encapsulated part is controlled by both V_{bg} and V_{tg}. This clearly resulted in four quadrants representing different p/n junction configurations [32] as indicated in Fig. 3(a). Due to the novelty of our device fabrication we could see four quadrants compared to the similar geometry reported in Refs. [20,21]. The nontopgated graphene regions in Refs. [20,21] are highly n doped by the polycarbonate. However, in our case, graphene in the topgated region as well as the nontopgated region is protected by the thin hBN and is not doped by polymers. So, we are also able to access the p-doped characteristics of the nontopgated regions.

A strong dependence of the spin relaxation time (τ_s) among the four junction configurations is observed as shown in Fig. 3(b). On average, the relaxation time is increased when the $n(n')$-doped region changes to $p(p')$-doped region. This can be observed at different topgate voltages as we move from n-n'-n region to n-p'-n region, and further to p-p'-p region. A possible explanation for the observed behavior is that the contacts can induce a slight doping, as can be seen from the asymmetric square resistance of graphene in Fig. 1(c). This might result in an additional p-n interface in the p-doped regime, decoupling the contacts from the channel and resulting in higher spin relaxation time for holes. Furthermore, the gate dependence of spin lifetime in Fig. 3(b) does not show a dip around the CNP [20,33] possibly due to the influence of p-n junctions formed at the edges of the topgated graphene channel near the CNP.

IV. CONCLUSIONS

In conclusion, we demonstrate a fully hBN encapsulated graphene device for spintronics applications. We show that the full encapsulation of graphene results in homogeneous charge and spin transport properties at room temperature. Charge transport measurements show uniform mobility across different regions of the encapsulated graphene. Spin transport measurements show that a uniform spin relaxation length across different channel regions is achieved with the crystalline hBN encapsulation. Further, our device shows spin transport across the whole thin-hBN encapsulated region of 12.5-μm length even in the presence of conductivity mismatch electrodes, demonstrating the potential of using hBN as a tunnel barrier for graphene spintronics. The dual gate geometry allowed us to study the effect of electric field on the spin transport. However, we do not observe a significant dependence due to the low values of achieved electric field. Moreover, we observe a strong dependence of the spin relaxation time on different p/n junction configurations. Further investigation is necessary to explain this behavior.

[1] A. H. Castro Neto, F. Guinea, N. M. R. Peres, K. S. Novoselov, and A. K. Geim, Rev. Mod. Phys. **81**, 109 (2009).

[2] S. Das Sarma, S. Adam, E. H. Hwang, and E. Rossi, Rev. Mod. Phys. **83**, 407 (2011).

[3] V. K. Dugaev, E. Y. Sherman, and J. Barnaś, Phys. Rev. B **83**, 085306 (2011).

[4] H. Min, J. E. Hill, N. A. Sinitsyn, B. R. Sahu, L. Kleinman, and A. H. MacDonald, Phys. Rev. B **74**, 165310 (2006).

[5] D. Pesin and A. H. MacDonald, Nat. Mater. **11**, 409 (2012).

[6] M. Drogeler, C. Franzen, F. Volmer, T. Pohlmann, L. Banszerus, M. Wolter, K. Watanabe, T. Taniguchi, C. Stampfer, and B. Beschoten, arXiv:1602.02725.

[7] S. Roche and S. O. Valenzuela, J. Phys. D: Appl. Phys. **47**, 094011 (2014).

[8] L. Wang, I. Meric, P. Y. Huang, Q. Gao, Y. Gao, H. Tran, T. Taniguchi, K. Watanabe, L. M. Campos, D. A. Muller, J. Guo, P. Kim, J. Hone, K. L. Shepard, and C. R. Dean, Science **342**, 614 (2013).

[9] P. J. Zomer, M. H. D. Guimaraes, N. Tombros, and B. J. van Wees, Phys. Rev. B **86**, 161416 (2012).

[10] D. Van Tuan, F. Ortmann, A. W. Cummings, D. Soriano, and S. Roche, Sci. Rep. **6**, 21046 (2016).

[11] A. V. Kretinin, Y. Cao, J. S. Tu, G. L. Yu, R. Jalil, K. S. Novoselov, S. J. Haigh, A. Gholinia, A. Mishchenko, M. Lozada, T. Georgiou, C. R. Woods, F. Withers, P. Blake, G. Eda, A. Wirsig, C. Hucho, K. Watanabe, T. Taniguchi, A. K. Geim, and R. V. Gorbachev, Nano Lett. **14**, 3270 (2014).

[12] F. Volmer, M. Drögeler, E. Maynicke, N. von den Driesch, M. L. Boschen, G. Güntherodt, C. Stampfer, and B. Beschoten, Phys. Rev. B **90**, 165403 (2014).

[13] G.-H. Lee, Y.-J. Yu, C. Lee, C. Dean, K. L. Shepard, P. Kim, and J. Hone, Appl. Phys. Lett. **99**, 243114 (2011).

[14] L. Britnell, R. V. Gorbachev, R. Jalil, B. D. Belle, F. Schedin, M. I. Katsnelson, L. Eaves, S. V. Morozov, A. S. Mayorov, N. M. R. Peres, A. H. C. Neto, J. Leist, A. K. Geim, L. A. Ponomarenko, and K. S. Novoselov, Nano Lett. **12**, 1707 (2012).

[15] Q. Wu, L. Shen, Z. Bai, M. Zeng, M. Yang, Z. Huang, and Y. P. Feng, Phys. Rev. Appl. **2**, 044008 (2014).

[16] T. Yamaguchi, Y. Inoue, S. Masubuchi, S. Morikawa, M. Onuki, K. Watanabe, T. Taniguchi, R. Moriya, and T. Machida, Appl. Phys. Express **6**, 073001 (2013).

[17] M. V. Kamalakar, A. Dankert, J. Bergsten, T. Ive, and S. P. Dash, Sci. Rep. **4**, 6146 (2014).

[18] W. Fu, P. Makk, R. Maurand, M. Bräuninger, and C. Schönenberger, J. Appl. Phys. **116**, 074306 (2014).

[19] P. J. Zomer, M. H. D. Guimares, J. C. Brant, N. Tombros, and B. J. v. Wees, Appl. Phys. Lett. **105**, 013101 (2014).

[20] M. H. D. Guimaraes, P. J. Zomer, J. Ingla-Aynes, J. C. Brant, N. Tombros, and B. J. van Wees, Phys. Rev. Lett. **113**, 086602 (2014).

[21] J. Ingla-Aynés, M. H. D. Guimarães, R. J. Meijerink, P. J. Zomer, and B. J. van Wees, Phys. Rev. B **92**, 201410 (2015).

[22] M. H. D. Guimares, A. Veligura, P. J. Zomer, T. Maassen, I. J. Vera-Marun, N. Tombros, and B. J. van Wees, Nano Lett. **12**, 3512 (2012).

[23] P. Blake, E. W. Hill, A. H. Castro Neto, K. S. Novoselov, D. Jiang, R. Yang, T. J. Booth, and A. K. Geim, Appl. Phys. Lett. **91**, 063124 (2007).

[24] R. V. Gorbachev, I. Riaz, R. R. Nair, R. Jalil, L. Britnell, B. D. Belle, E. W. Hill, K. S. Novoselov, K. Watanabe, T. Taniguchi, A. K. Geim, and P. Blake, Small **7**, 465 (2011).

[25] N. Tombros, C. Jozsa, M. Popinciuc, H. T. Jonkman, and B. J. van Wees, Nature (London) **448**, 571 (2007).

[26] S. V. Morozov, K. S. Novoselov, M. I. Katsnelson, F. Schedin, D. C. Elias, J. A. Jaszczak, and A. K. Geim, Phys. Rev. Lett. **100**, 016602 (2008).

[27] P. J. Zomer, S. P. Dash, N. Tombros, and B. J. van Wees, Appl. Phys. Lett. **99**, 232104 (2011).

[28] T. Maassen, I. J. Vera-Marun, M. H. D. Guimarães, and B. J. van Wees, Phys. Rev. B **86**, 235408 (2012).

[29] W. Han, K. Pi, K. M. McCreary, Y. Li, J. J. I. Wong, A. G. Swartz, and R. K. Kawakami, Phys. Rev. Lett. **105**, 167202 (2010).

[30] Y. W. Huang, C. K. Lo, Y. D. Yao, L. C. Hsieh, and J. H. Huang, J. Appl. Phys. **97**, 10D504 (2005).

[31] Y. Zhang, T.-T. Tang, C. Girit, Z. Hao, M. C. Martin, A. Zettl, M. F. Crommie, Y. R. Shen, and F. Wang, Nature (London) **459**, 820 (2009).

[32] J. R. Williams, L. DiCarlo, and C. M. Marcus, Science **317**, 638 (2007).

[33] W. Han and R. K. Kawakami, Phys. Rev. Lett. **107**, 047207 (2011).